Journal of Power Sources 267 (2014) 682–691

Contents lists available at ScienceDirect

Journal of Power Sources

journal homepage: www.elsevier.com/locate/jpowsour

Cerium fluoride coated layered oxide $Li_{1.2}Mn_{0.54}Ni_{0.13}Co_{0.13}O_2$ as cathode materials with improved electrochemical performance for lithium ion batteries

Chao Lu, Hao Wu*, Yun Zhang*, Heng Liu, Baojun Chen, Naiteng Wu, Sen Wang

College of Materials Science and Engineering, Sichuan University, Chengdu 610064, China

HIGHLIGHTS

- Cerium fluoride is used as a novel coating material for Li-rich layered cathode.
- Coated cathode displays enhanced high-rate capability and cycling stability.
- Coating layer suppresses the increase of electrochemical impedance of electrode.

ARTICLE INFO

Article history:
Received 3 April 2014
Received in revised form
21 May 2014
Accepted 22 May 2014
Available online 5 June 2014

Keywords:
Cerium fluoride
Lithium-rich cathode material
Layered oxides
Surface coating
Lithium ion battery

ABSTRACT

Cerium fluoride (CeF_3) coated lithium-rich layered $Li_{1.2}Mn_{0.54}Ni_{0.13}Co_{0.13}O_2$ particles are synthesized using a facile chemical deposition route. The structural and electrochemical properties of pristine and CeF_3-coated electrodes are investigated by X-ray diffraction (XRD), thermogravimetric-differential scanning calorimetry (TG-DSC), scanning electron microscopy (SEM), energy dispersive spectroscopy (EDS), transmission electron microscopy (TEM), galvanostatic charge/discharge tests, electrochemical impedance spectra (EIS) and cyclic voltammetry (CV). The results indicate that the cathode particles are uniformly covered with a CeF_3 layer (~10 nm thick) after 2 wt.% CeF_3 surface coating. The coated electrode shows an enhanced initial coulombic efficiency of 80.8% compared to 75.2% for the pristine electrode. Moreover, the coated electrode demonstrates better cyclic performance, which exhibits capacity retention of 91.7% after 50 cycles compared with only 82.1% for the pristine one. Furthermore, the CeF_3-coated electrode delivers a superior high-rate capacity of 103.1 mAh g^{-1} at 5C, higher than 82.2 mAh g^{-1} for the pristine one. The remarkably improved cycling stability and high-rate capacity of the surface-modified electrode is ascribed to the presence of a stable and thin CeF_3 coating layer which effectively reduces the damage of electrode structure and suppresses the increase of impedance during cycling by preventing direct contact of electrode with electrolyte.

1. Introduction

Lithium ion batteries (LIBs) are gaining more interest due to the ever-growing demands for energy storage and supply. Development of safety, low-cost, long lifetime, high energy density and power density are the critical issues for the practical application of LIBs. Li-containing oxides are the traditional cathode materials for LIBs such as $LiCoO_2$ [1], spinel $LiMn_2O_4$ [2], and olivine $LiFePO_4$ [3], and some of them have been indeed commercialized. However, utilization of these cathode materials still cannot satisfy the requirements for high-power LIBs used in electric vehicles (EVs) and hybrid electric vehicles (HEVs). For example, layered $LiCoO_2$ as the cathode materials always exhibits a limited practical capacity of ~140 mAh g^{-1} due to chemical and structural instabilities at deep charge. Olivine $LiFePO_4$ has intrinsically low electronic conductivity (~10^{-9}–10^{-10} S cm^{-1}) [4] and low Li^+ diffusion rate (~10^{-14}–10^{-16} cm^2 s^{-1}) [5], which significantly restrict their high rate capability of fast charging and discharging, resulting in a poor power performance.

As an alternative to these traditional cathode materials, the solid solution series of layered structure oxides with the composition of $Li_2MnO_3 \cdot LiMO_2$ (M = Ni, Co, Mn or combinations) have recently appealed growing interest [6–9]. Such Li-rich layered oxides can

* Corresponding authors. Sichuan University, 24, South Section 1, Yihuan Road, Chengdu 610065, Sichuan, PR China. Tel./fax: +86 028 85410272.
E-mail addresses: hao.wu@scu.edu.cn (H. Wu), y_zhang@scu.edu.cn (Y. Zhang).

http://dx.doi.org/10.1016/j.jpowsour.2014.05.122
0378-7753/

deliver an extraordinarily high theoretical discharge capacity of more than 250 mAh g^{-1} and possess high operating potential of 4.6–4.8 V (vs. Li/Li^+) [10–14], which shows a great potential in application for EVs and HEVs. However, when charged up to 4.6 V, the Li-rich layered cathode materials always undergo a huge irreversible capacity loss of 40–100 mAh g^{-1} in the first cycle depending on the composition. The irreversible capacity loss is attributed to the extraction of lithium as "Li_2O" from the inert Li_2MnO_3 concomitant with an irreversible elimination of oxygen vacancies from the lattice [15–17], which leads to fewer intercalation active sites for lithium ions after the first charge. As a result, there is a significant difference between the first charge and discharge capacity values. In addition, the relatively high operating voltage (up to 4.6 V) can accelerate the dissolution of transition metal Mn element from cathodes in contact with electrolyte, which results in a steady capacity decay during the electrochemical cycling process.

Surface coating or modification has been testified to be an effective approach to improve the electrochemical performance of cathode materials for LIBs when they are charged at a high cut-off potential or cycled for a long time. To date, metal oxides including Al_2O_3 [18], TiO_2 [19], ZnO [20], MgO [21], ZrO_2 [22] have been extensively used as coating materials for improving the electrochemical performance of cathodes. The coating materials can serve as a protective layer to prevent the cathode active particles from direct contact with electrolyte, thus suppressing the decomposition of active materials at high operating voltage and improving the electrochemical performance ultimately. In the case of Al_2O_3 coating layer, for instance, Al_2O_3 scavenged HF species from the hydrolysis of electrolyte with a trace amount of water and formed chemically stable aluminum fluoride layers which could result in less decomposition of the cathode particles during the electrochemical cycling [23–26]. This fact implies that the metal fluoride is also able to be a promising candidate of coating materials for fabricating cathodes with enhanced electrochemical performance.

Recently, cerium oxide has been found to be an effective coating material for improving the electrochemical performance of cathode materials [27–30]. Ha et al. [31] reported that the enhanced electrochemical properties and cycling stability of CeO_2-coated $LiNi_{0.8}Co_{0.2}O_2$ were due to the fact that CeO_2 coating layer can suppress the phase structure transformation of $LiNi_{0.8}Co_{0.2}O_2$ and promote its thermal stability. Compared with CeO_2, cerium fluoride (CeF_3) particles are chemically inert at high temperature (up to 923 K) [32], and have better structural stability in acidic environment such as HF-containing electrolyte solution. Furthermore, CeF_3 has been reported to have high ionic conductivity at room temperature [33,34]. These facts allow to use CeF_3 as a promising coating material for the surface modification of electrodes. However, to our best knowledge, there is no report regarding the use of cerium fluorides for cathode surface-coating up to now. Herein, we report for the first time to introduce CeF_3 as an effective coating material for the surface-modification of Li-rich layered oxides, and aim to obtain CeF_3-coated cathodes with enhanced rate capability and cycling performance for LIBs.

In this paper, Li-rich layered oxide, $Li_{1.2}Mn_{0.54}Ni_{0.13}Co_{0.13}O_2$, was first prepared, followed by successful coating with a small amount of CeF_3 using simple chemical deposition method. It was found that the surface coating by CeF_3 obviously improved the initial coulombic efficiency, the rate capability and the cyclic performance of the cathode material for LIBs. A detailed explanation regarding the effects of CeF_3-coating on the structure and electrochemical properties of the cathode material was also discussed.

2. Experimental

2.1. Preparation of samples

The pristine layered oxide $Li_{1.2}Mn_{0.54}Ni_{0.13}Co_{0.13}O_2$ powders were prepared by co-precipitation method. At first, stoichiometric amounts of $NiSO_4 \cdot 6H_2O$, $CoSO_4 \cdot 7H_2O$, and $MnSO_4 \cdot H_2O$ were dissolved together in distilled water to get a transparent solution. Then, a mixed solution containing NaOH and NH_4OH was added to the transition metal sulfate solution drip by drip, followed by vigorously stirring for 1 h to get the metal hydroxide $Mn_{0.675}Ni_{0.1625}Co_{0.1625}(OH)_2$. After thoroughly washing with deionized water and vacuum drying, the obtained metal hydroxides were mixed with 3 wt.% excess $LiOH \cdot H_2O$, followed by grinding in a ball mill. Finally, the mixture was calcined at 900 °C for 12 h in air to obtain the target compound of $Li[Li_{0.2}Mn_{0.54}Ni_{0.13}Co_{0.13}]O_2$ powders.

To prepare CeF_3-coated $Li[Li_{0.2}Mn_{0.54}Ni_{0.13}Co_{0.13}]O_2$, the as-prepared cathode powders was immersed into the $Ce(NO_3)_3$ aqueous solution under continuous stirring, followed by dripping NH_4F solution into the suspension solution. The molar ratio of F to Ce element was regulated to 3:1 and the coating amount of CeF_3 was set to 2 wt.% of the parent cathode material. Afterward, the suspension solution was heated at 80 °C slowly until the solvent was completely evaporated. The dried powders was further heated in air at 450 °C for 2 h to get the CeF_3-coated $Li[Li_{0.2}Mn_{0.54}Ni_{0.13}Co_{0.13}]O_2$.

2.2. Characterizations

The crystalline structure of samples was characterized by X-ray diffraction (XRD) using a Bruker DX-1000 diffractometer with Cu kα radiation in the 2θ angular range of 10°–80° at a scanning rate of 0.02° s^{-1}. Thermal analysis of the CeF_3-coated electrode was carried out by using a simultaneous thermal analyzer (TG-DSC, STA 449C, Netzsch, Germany) in the temperature range of 40 °C–450 °C in air at a heating rate of 10 °C min^{-1}. The particle morphology and element composition of the powders were observed by using scanning electron microscope (SEM, Hitachi S-4800) equipped with energy dispersive spectroscope (EDS). Transmission electron microscope (TEM, JEOL JEM-100CX) was used to examine the coating layer of cathode powders at an acceleration voltage of 80 kV. The microstructure of the coated cathode particles was observed by employing high resolution transmission electron microscope (HRTEM, JEOL JEM-2100F).

2.3. Electrochemical measurements

The working electrodes were fabricated by dispersing 80 wt.% $Li[Li_{0.2}Mn_{0.54}Ni_{0.13}Co_{0.13}]O_2$ powders (active materials), 15 wt.% carbon black (conductive agent), and 5 wt.% polyvinylidene fluoride (PVDF, binder) in *N*-methyl-2-pyrrolidone (NMP) solvent to form a homogeneous slurry, followed by plastering the slurry onto aluminum foil current collector and dried at 120 °C overnight in a vacuum oven. All electrodes were cut into disks with a diameter of 1.4 cm, the average mass loading of which was about 2.0 mg cm^{-2}. For electrochemical measurements, CR-2032 coin-type cells were assembled in an argon-filled glove box by utilizing the above prepared disks as cathode, metal lithium foils as anode, polypropylene micro-porous films (Celgard 2400) as separator, and 1.0 mol L^{-1} $LiPF_6$ dissolved in a mixture of ethylene carbonate (EC) and dimethyl carbonate (DMC) and diethyl carbonate (DEC) (1:1:1 in volume) as electrolyte. The galvanostatic charge and discharge tests of the cells were performed on a Neware program-control test system (Shen Zhen, CT-3008W) in the potential range between 2.0

and 4.6 V at different current densities from 25 mA g^{-1} (0.1C) to 1250 mA g^{-1} (5C). The electrochemical impedance spectra (EIS) were carried out in the frequency range from 100 kHz to 10 mHz with an a.c. amplitude of 5 mV using VMP3 (France, SN 0746). The cyclic voltammogram (CV) measurements were conducted on the same instrument in the voltage range of 2.0–4.6 V at a scanning rate of 0.1 mV s^{-1}.

3. Results and discussion

The XRD patterns and Miller indices of the pristine Li[$Li_{0.2}Mn_{0.54}Ni_{0.13}Co_{0.13}$]$O_2$ and CeF_3-coated Li[$Li_{0.2}Mn_{0.54}Ni_{0.13}Co_{0.13}$]$O_2$ are shown in Fig. 1. The weak superlattice peaks between 20° and 25° are indexed to the monoclinic Li_2MnO_3-like domains with space group symmetry of C2/m, and the other diffraction patterns of both samples can be identified as the α-$NaFeO_2$ hexagonal structure with space group R-3m (high symmetry). Additionally, no peak for any impurity phase is detected in the XRD patterns. Furthermore, the clear splitting of (006)/(012) and (018)/(110) demonstrates that a highly ordered layered hexagonal structure is obtained. The integrated ratio of $I_{(003)}/I_{(104)}$ peaks, an important indication of the cation mixing between Li^+ and Ni^{2+} of which the radii are similar [35], is calculated as 1.45 (>1.2), also confirming well formation of layered structure evidently. Due to the low concentration and/or the amorphous state of CeF_3 after calcination treatment at 450 °C, no observable diffraction peak corresponding to crystalline CeF_3 is detected for the CeF_3-coated Li[$Li_{0.2}Mn_{0.54}Ni_{0.13}Co_{0.13}$]$O_2$. It is believed that the parameter "a" corresponds to the average distance between metal and oxygen, and any variation of the parameter suggests the diffusion of foreign ions into the bulk structure of host material [22]. The refined lattice parameters of the CeF_3-coated Li[$Li_{0.2}Mn_{0.54}Ni_{0.13}Co_{0.13}$]$O_2$ are calculated as a = 2.855 Å, c = 14.228 Å, which are almost identical to that of the pristine electrode (a = 2.854 Å, c = 14.238 Å), indicating that there is no obvious structural change in the Li[$Li_{0.2}Mn_{0.54}Ni_{0.13}Co_{0.13}$]$O_2$ electrode after coating.

In order to confirm the presence of amorphous cerium fluoride on electrode surface, we calcined 8 wt.% CeF_3 coated electrode under nitrogen flow at 450 °C and 600 °C, respectively. As shown in Fig. 2a, no any diffraction peak regarding CeF_3 can be seen at 450 °C even though the coating amount of fluoride reached 8 wt.% of the host material. However, low intensity characteristic peaks corresponding to crystalline CeF_3 (PDF#08-0045) appear in the XRD pattern of 8 wt.% fluoride-coated electrode when calcinated at an elevated temperature of 600 °C (Fig. 2b). This result implies that the calcination temperature of 450 °C is too low to achieve full crystallization of the cerium fluoride. Accordingly, it can be concluded that the cerium fluoride is indeed present in an amorphous phase on the surface of the layered oxide electrode when the coated electrode is thermally treated at 450 °C.

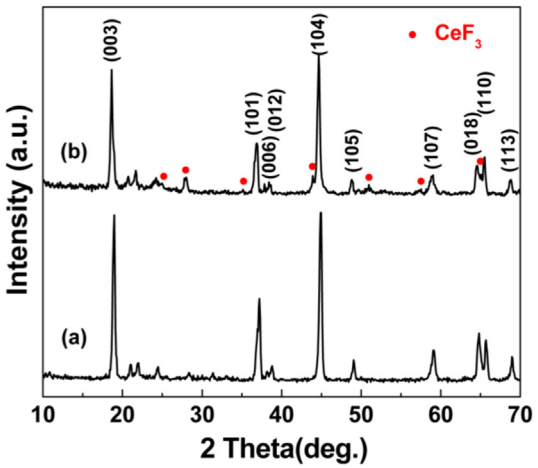

Fig. 2. XRD patterns of 8 wt.% CeF_3-coated Li[$Li_{0.2}Mn_{0.54}Ni_{0.13}Co_{0.13}$]$O_2$ heated at (a) 450 °C and (b) 600 °C under nitrogen flow.

Fig. 3 shows the TG-DSC results for the 2 wt.% fluoride-coated Li[$Li_{0.2}Mn_{0.54}Ni_{0.13}Co_{0.13}$]$O_2$ electrode calcinated at 450 °C in air. The weight loss of about 2.8% was observed at temperature lower than 100 °C. The sharp endothermic peaks at about 72 °C and 100 °C in DSC profile, corresponding to the mass loss in TG profile, are mainly attributed to the removal of moisture from the coated electrode. From the range of 100 °C–450 °C, one can see that the weight of coated electrode remains almost unchanged, whilst several endothermic peaks appear between 100 °C and 450 °C, which is associated to the decomposition and volatilization of ammonium nitrate generated during the coating process. It should be noted that there is no endothermic peak referring to formation of crystalline CeF_3 in such a temperature range. The TG/DSC test results coincide with the above-mentioned XRD analyses.

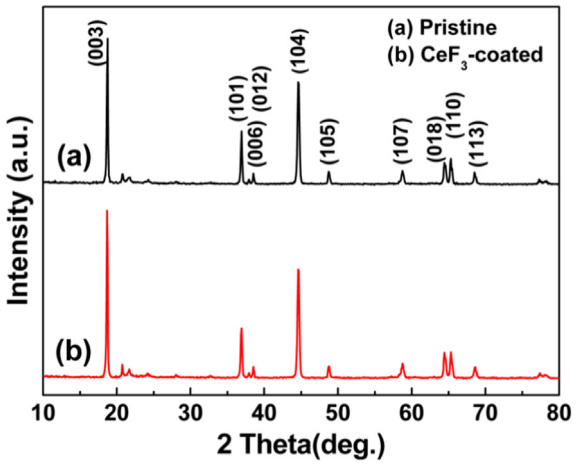

Fig. 1. XRD patterns of (a) pristine and (b) 2 wt.% CeF_3-coated Li[$Li_{0.2}Mn_{0.54}Ni_{0.13}Co_{0.13}$]$O_2$.

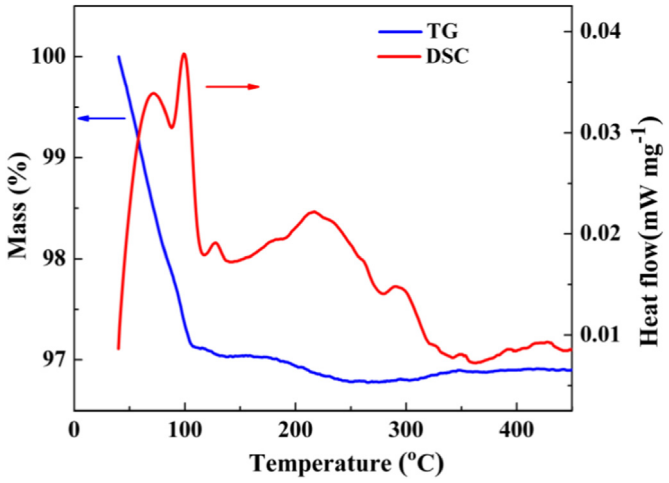

Fig. 3. TG-DSC profiles of the 2 wt.% CeF_3-coated Li[$Li_{0.2}Mn_{0.54}Ni_{0.13}Co_{0.13}$]$O_2$ heated between 40 °C and 450 °C.

Fig. 4 presents the SEM images of the pristine $Li[Li_{0.2}Mn_{0.54}Ni_{0.13}Co_{0.13}]O_2$ and CeF_3-coated $Li[Li_{0.2}Mn_{0.54}Ni_{0.13}Co_{0.13}]O_2$. It can be seen that both samples have similar surface morphologies and saturated primary particles with a size of 200–600 nm. The reason for the indistinct morphology difference between the two electrodes is mainly due to the relatively low coating amount (2 wt.%) of CeF_3. It should be noted that there are a lot of tiny dots distributed on the particle surface of both pristine and CeF_3-coated $Li[Li_{0.2}Mn_{0.54}Ni_{0.13}Co_{0.13}]O_2$, which can be reasonably attributed to the deposition of sprayed gold particles generally used to enhance the conductivity of electrodes for SEM measurement.

The surface morphologies and microstructure for both samples are further analyzed by typical transmission electron microscope (TEM) and high resolution TEM (HRTEM) observations, respectively, as shown in Fig. 5. The pristine $Li[Li_{0.2}Mn_{0.54}Ni_{0.13}Co_{0.13}]O_2$ particles (Fig. 5a) have smooth edge lines without any coating layers, whereas the CeF_3-coated $Li[Li_{0.2}Mn_{0.54}Ni_{0.13}Co_{0.13}]O_2$ particles (Fig. 5b) are covered with a thin layer of about 10 nm in thickness. Compared with the compact core material, the coating layer possibly has a loosened and porous structure. It is expected that the presence of the coating layer with amorphous structure around the $Li[Li_{0.2}Mn_{0.54}Ni_{0.13}Co_{0.13}]O_2$ particles will lower the surface activity by reducing the contact area with the electrolyte and facilitate the transport of lithium ions across the surface due to its porous structure, thereby improving the electrochemical performance of the layered oxides. As for the HRTEM image in Fig. 5c, it is clearly noted that the interplanar distance of the CeF_3-coated $Li[Li_{0.2}Mn_{0.54}Ni_{0.13}Co_{0.13}]O_2$ is 0.471 nm, in consistent with the distance between the lattice fringes in the typical (003) crystal plane of the layered R-3m phase belonging to the $Li[Li_{0.2}Mn_{0.54}Ni_{0.13}Co_{0.13}]O_2$ [24,36], which confirms that the core material of the CeF_3-coated sample still maintains an intact hexagonal ordering structure after surface modification. However, no lattice fringes corresponding to crystal CeF_3 are observed in the HRTEM image, indicating that the fluoride coating layer is probably in an amorphous phase on the cathode surface.

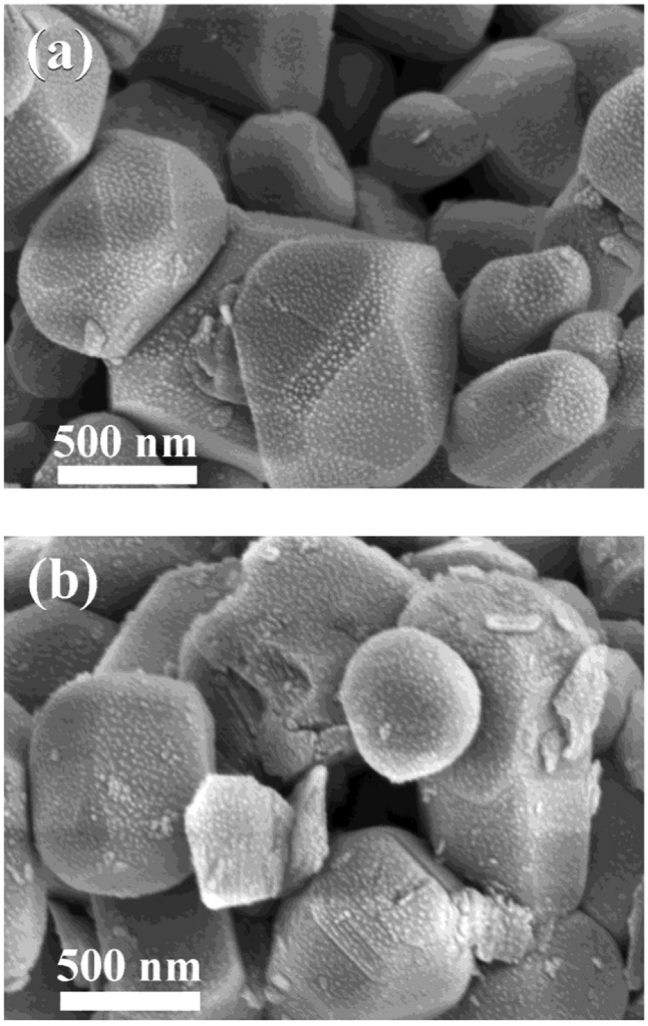

Fig. 4. SEM images of (a) $Li[Li_{0.2}Mn_{0.54}Ni_{0.13}Co_{0.13}]O_2$ and (b) 2 wt.% CeF_3-coated $Li[Li_{0.2}Mn_{0.54}Ni_{0.13}Co_{0.13}]O_2$.

In order to further confirm the uniform coating of CeF_3 on the surface of lithium-rich layered oxide, EDS analysis is carried out and the results are shown in Fig. 6. The energy dispersive spectrum (Fig. 6b) directly illustrates the presence of both Ce and F on the surface of $Li[Li_{0.2}Mn_{0.54}Ni_{0.13}Co_{0.13}]O_2$ particles. The EDS elemental mapping images, as shown in Fig. 6c–h, clearly demonstrate that the Ce element and F element are both homogeneously distributed on the surface of cathode particles.

The electrochemical properties of the samples were evaluated by using a coin-type cell. The initial galvanostatic charge–discharge profiles of the bare $Li[Li_{0.2}Mn_{0.54}Ni_{0.13}Co_{0.13}]O_2$ and CeF_3-coated $Li[Li_{0.2}Mn_{0.54}Ni_{0.13}Co_{0.13}]O_2$ at a constant current density of 0.1C rate ($1C = 250\ mA\ g^{-1}$) between 2.0 and 4.6 V are shown in Fig. 7. It is noticeably shown that both of the electrodes exhibit a long voltage plateau at about 4.55 V during the initial charging process, demonstrating a typical feature of the lithium-rich layered oxides written as $Li_2MnO_3 \cdot LiMnO_2$ (M = Ni, Co or Mn). Generally, the first charging process for the layered $Li_2MnO_3 \cdot LiMO_2$ can be divided into two steps [37]. The first step of charging process exists in the potential region between 3 V and 4.4 V, which is directly related to the lithium extraction from the layered $LiMO_2$ component, accompanying with the oxidation of Ni^{2+} to Ni^{4+} and Co^{3+} to Co^{4+}. For the second step, when charged above 4.5 V, the irreversible lithium ion extraction and oxygen release from the monoclinic Li_2MnO_3-like domains are significantly responsible for the activation of Li_2MnO_3 region and the formation of electrochemically active component MnO_2. The corresponding reaction mechanism of the above two charging process can be explained as follows.

$$LiMO_2 \rightarrow MO_2 + Li^+ + e^- \quad (1)$$

$$Li_2MnO_3 \rightarrow MnO_2 + 2Li^+ + 1/2O_2 + 2e^- \quad (2)$$

Interestingly, in addition to the capacity contribution arising from the layered $LiMO_2$ component, this active product MnO_2, in which lithium ions can be intercalated and de-intercalated reversibly, can provides extra discharge capacity at high operating voltage. As shown in Fig. 7, the pristine electrode presents a longer voltage plateau than the CeF_3-coated one, suggesting that the obtained charge capacity for the CeF_3-coated sample is relatively smaller than that for the pristine sample. This can be probably ascribed that the strong interaction of F–O bonds by surface fluorination suppresses the migration of oxygen vacancies and reduces the activity of evolved oxygen [17]. Moreover, the inhibition effect from the CeF_3 thin layer further slows down the activation of the cathode material during the first charge, which consequently leads to the slightly lower discharge capacity of the CeF_3-coated electrode after the first discharge, as seen in Fig. 7. The initial charge and discharge capacities are 304.6 mAh g^{-1}, 229.0 mAh g^{-1} and 275.8 mAh g^{-1}, 222.8 mAh g^{-1} for the pristine and CeF_3-coated $Li[Li_{0.2}Mn_{0.54}Ni_{0.13}Co_{0.13}]O_2$ electrodes, respectively, corresponding to the coulombic efficiency of 75.2% and 80.8%, respectively. Although the discharge capacity of the CeF_3-coated electrode is

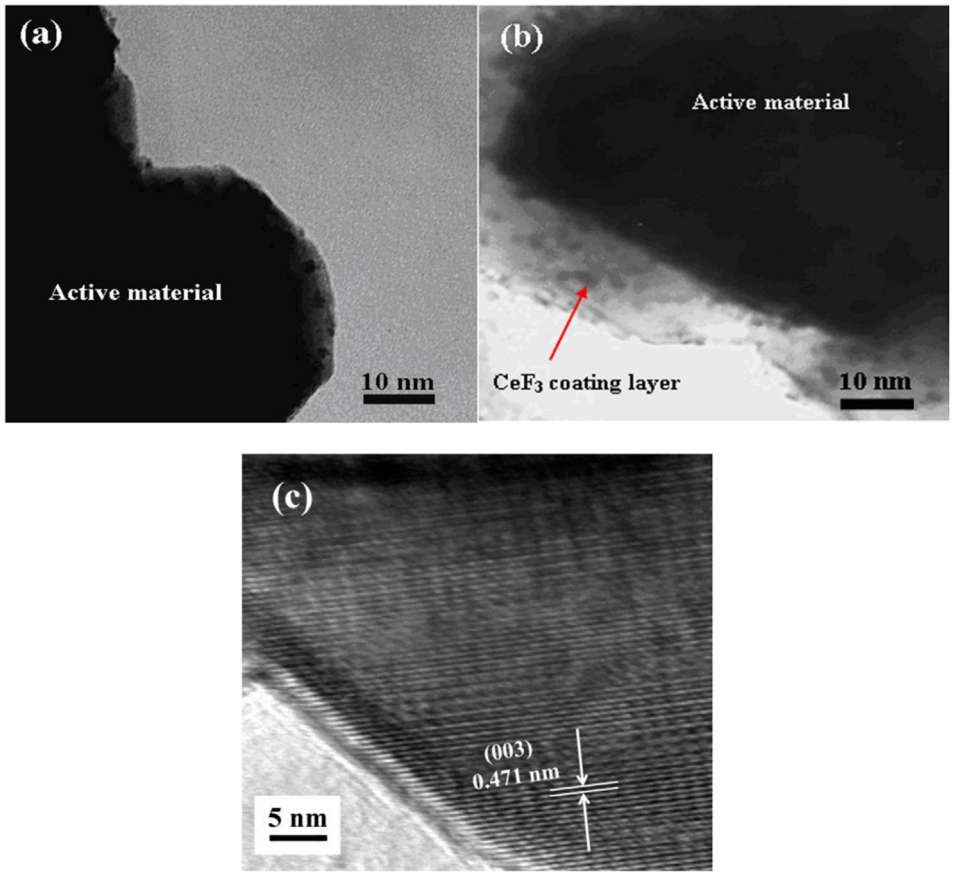

Fig. 5. TEM images of (a) $Li[Li_{0.2}Mn_{0.54}Ni_{0.13}Co_{0.13}]O_2$ and (b) 2 wt.% CeF_3-coated $Li[Li_{0.2}Mn_{0.54}Ni_{0.13}Co_{0.13}]O_2$; (c) HRTEM image of 2 wt.% CeF_3-coated $Li[Li_{0.2}Mn_{0.54}Ni_{0.13}Co_{0.13}]O_2$.

slightly lower than that of the pristine one, the CeF_3-coated cathode exhibits a smaller irreversible capacity loss of 53.0 mAh g^{-1} compared to that (75.6 mAh g^{-1}) of the pristine. This value of capacity loss for CeF_3-coated cathode is close to or lower than those of other oxide-coated cathodes for LIBs such as 54.0 mAh g^{-1} for 9 wt.% TiO_2-coated $Li[Li_{0.2}Mn_{0.54}Ni_{0.13}Co_{0.13}]O_2$ [38], 71.3 mAh g^{-1} for 2 wt.% ZrO_2-coated $Li[Li_{0.2}Mn_{0.54}Ni_{0.13}Co_{0.13}]O_2$ [22]. The main reason of the relatively lower irreversible capacity loss and higher initial coulombic efficiency for the CeF_3-coated cathode can be attributed to the suppression of the oxidation of the electrolyte and the dissolution of the transition metals as a result of the successful surface coating with CeF_3. This fact demonstrates that CeF_3 coating on the surface of $Li[Li_{0.2}Mn_{0.54}Ni_{0.13}Co_{0.13}]O_2$ electrode effectively enhances the initial coulombic efficiency.

Fig. 8 compares the discharge capacity as a function of cycle number for the $Li[Li_{0.2}Mn_{0.54}Ni_{0.13}Co_{0.13}]O_2$ and CeF_3-coated $Li[Li_{0.2}Mn_{0.54}Ni_{0.13}Co_{0.13}]O_2$ electrode at a constant current density of 0.1C (25 mA g^{-1}) in a potential region between 2.0 and 4.6 V at 25 °C. Distinctly, the electrode coated with CeF_3 exhibits much better cyclic performance than the pristine electrode. The CeF_3-coated sample delivers higher discharge capacity than that of the pristine sample, except for the discharge capacity during the first 5 cycles. In the case of pristine cathode, it delivers an initial discharge capacity of 229.0 mAh g^{-1} with only 188.1 mAh g^{-1} reserved in the 50th cycle, corresponding to a capacity retention of 82.1%. The discharge capacity of the pristine sample drops rapidly in a linearly decreased trend, due to the annihilation of the temporary oxygen vacancies derived from the initial activation of inert Li_2MnO_3 component and the gradual sabotage of the bare particle surface by HF attack during the electrochemical cycling. On the contrary, the discharge capacity of the CeF_3-coated cathode keeps a slightly increased trend during the first 5 cycles, demonstrating that several cycles at a current density of 0.1C are essential to achieve adequate wetting contact between the solid electrode and aqueous electrolyte and induce complete activation of the Li_2MnO_3 phase after surface coating with CeF_3. Thus, it suggests that the activation of Li_2MnO_3 is delayed as a result of the CeF_3 coverage. Furthermore, the discharge capacity of CeF_3-coated electrode still retains as high as 204.5 mAh g^{-1} even after 50 electrochemical cycles, showing a capacity retention of 91.7% with respect to that of the initial cycle. The improved cyclic stability of CeF_3-coated electrode can be comparable to or better than Li_2TiF_6-coated $Li[Li_{0.2}Mn_{0.54}Ni_{0.13}Co_{0.13}]O_2$ electrode as reported in literature [39]. As we know, the higher the capacity retention, the better the cyclic stability for the electrode. The superior electrochemical cycling performance of the coated cathode can be mainly attributed to the presence of CeF_3 coating layer which not only generates effective suppression of the side reaction between the positive electrode and the electrolyte, but also avoids the fast decomposition of electrolyte and the drastic dissolution of transition metal ions (Mn and/or Ni) at high operating potential up to 4.6 V. Hence, it can be reasonable to speculate that the interface reaction on the surface of the active particles can be significantly restrained by CeF_3 coating layers, and consequently the electrochemical cycling performance of $Li[Li_{0.2}Mn_{0.54}Ni_{0.13}Co_{0.13}]O_2$ is ultimately improved.

The charge/discharge profiles for the pristine and CeF_3-coated electrodes during the 2nd, 10th, and 50th cycles at 0.2C are present in Fig. 9. As the cycle goes on, it is seen that the charge profiles move to higher voltage plateaus and the discharge profiles shift to lower voltage plateaus for both electrodes, implying the increase of

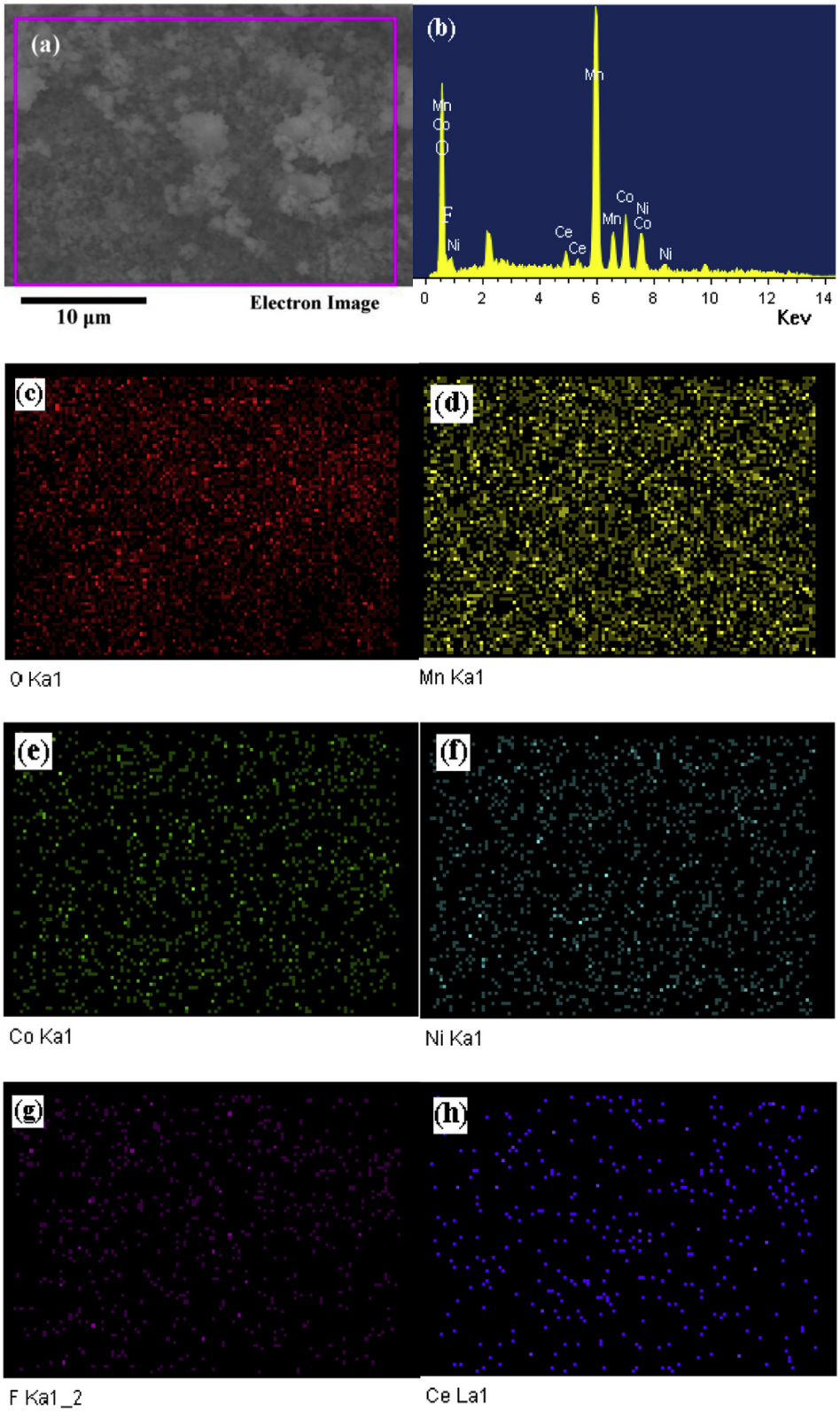

Fig. 6. SEM image (a), EDS spectrum (b) and EDS elemental mapping images [(c)–(h)] of 2 wt.% CeF_3-coated $Li[Li_{0.2}Mn_{0.54}Ni_{0.13}Co_{0.13}]O_2$ particles.

polarization with cycles. From the 2nd to 50th cycle, the discharge midpoint voltage of the pristine sample decreases from 3.28 V to 3.24 V (as indicated by the arrow), while that of the coated electrode reduces from 3.41 V to 3.36 V. We can also see that the charge and discharge capacities for the two electrodes in the 2nd and 10th cycles are close to each other, respectively, whereas major change occurs after 50 cycles. Compared with the discharge capacity of 174.7 mAh g^{-1} for the pristine $Li[Li_{0.2}Mn_{0.54}Ni_{0.13}Co_{0.13}]O_2$, the

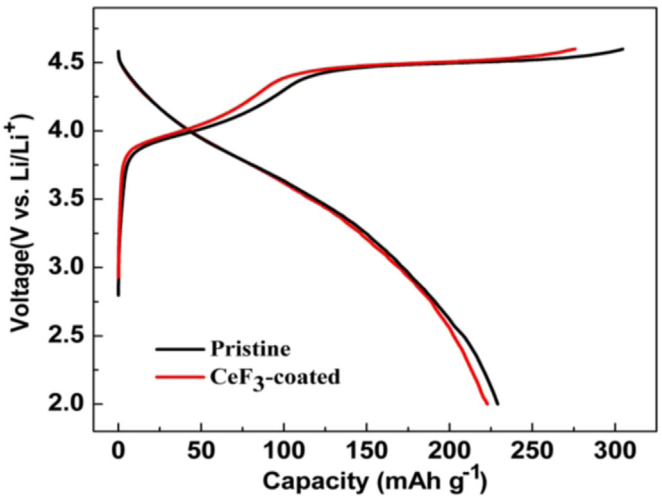

Fig. 7. The initial charge and discharge curves of the $Li[Li_{0.2}Mn_{0.54}Ni_{0.13}Co_{0.13}]O_2$ and CeF_3-coated $Li[Li_{0.2}Mn_{0.54}Ni_{0.13}Co_{0.13}]O_2$ electrodes over 2.0–4.6 V.

CeF_3-coated one delivers a capacity of 196.4 mAh g^{-1} in the 50th cycle. The smaller voltage decay and higher discharge capacity for the coated electrode after 50 cycles can be ascribed to the protection from CeF_3 coating layer which suppresses the electrode surface reaction with electrolyte solution and enhances the structural stability of cathode material.

Fig. 10 compares the rate capabilities of samples from 0.1C to 5C. Obviously, the CeF_3-coated sample shows better rate capability than the pristine one. As shown in Fig. 10a, the pristine cathode material delivers discharge capacities of 229.0 mAh g^{-1}, 195.9 mAh g^{-1}, 166.9 mAh g^{-1}, 136.1 mAh g^{-1} and 82.2 mAh g^{-1} at 0.1C, 0.5C, 1C, 2C and 5C current density, respectively. By contrast, the CeF_3-coated electrode exhibits discharge capacity of 222.9 mAh g^{-1}, 203.2 mAh g^{-1}, 175.0 mAh g^{-1}, 147.4 mAh g^{-1} and 103.1 mAh g^{-1} at the correspondingly increased current density. The improved high-rate (2C, 5C) discharge capacities for the 2 wt.% CeF_3-coated $Li[Li_{0.2}Mn_{0.54}Ni_{0.13}Co_{0.13}]O_2$ are higher than those (lower than 98.0 mAh g^{-1} at 2C and 49.0 mAh g^{-1} at 5C,

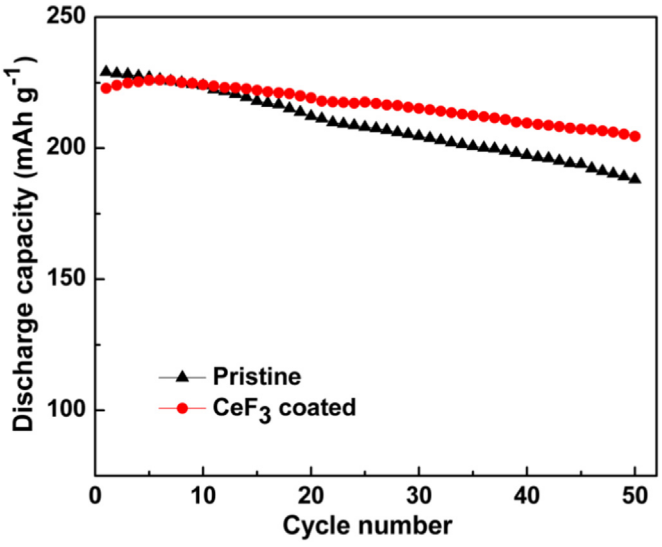

Fig. 8. Cyclic performance of the $Li[Li_{0.2}Mn_{0.54}Ni_{0.13}Co_{0.13}]O_2$ and CeF_3-coated $Li[Li_{0.2}Mn_{0.54}Ni_{0.13}Co_{0.13}]O_2$ electrodes during 50 cycles at a current density of 0.1C between 2.0 and 4.6 V.

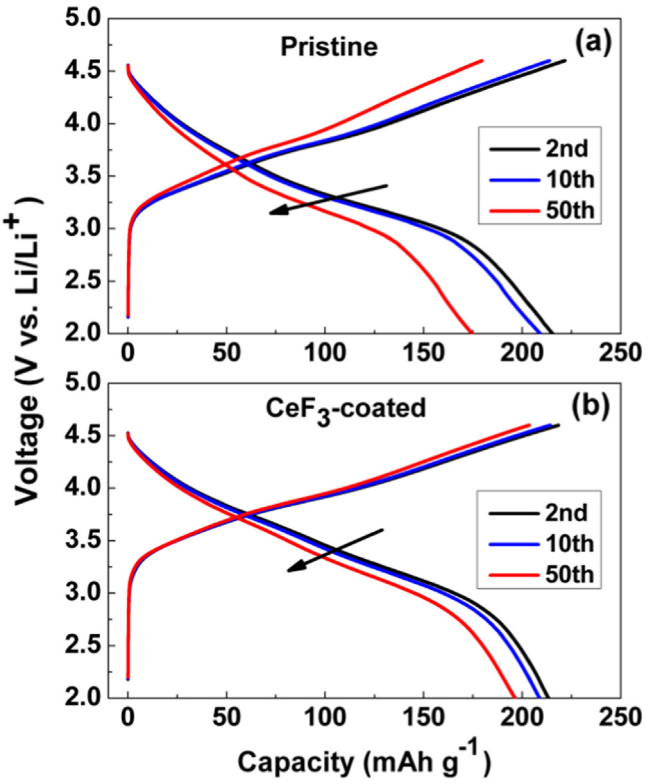

Fig. 9. The charge/discharge profiles for the pristine and CeF_3-coated $Li[Li_{0.2}Mn_{0.54}Ni_{0.13}Co_{0.13}]O_2$ in the 2nd, 10th, and 50th cycles at 0.2C rate.

respectively) for the ZnO, ZrO_2 or Al_2O_3-coated $Li[Li_{0.2}Mn_{0.54}Ni_{0.13}Co_{0.13}]O_2$ electrodes [40]. It should be noted that at high current densities (>0.1C), the discharge capacity of the coated sample is comparatively larger than that of the pristine one, illustrating that the CeF_3-coated $Li[Li_{0.2}Mn_{0.54}Ni_{0.13}Co_{0.13}]O_2$ is significantly more durable to higher discharge current than the uncoated parent cathode and an improved rate capability can be obtained by surface coating with CeF_3.

In order to get insight into the intrinsic effect of CeF_3 coating on the electrochemical performance of pristine $Li[Li_{0.2}Mn_{0.54}Ni_{0.13}Co_{0.13}]O_2$, electrochemical impedance spectroscopy (EIS) analysis is performed. The measurements are carried out at a fully charged state of 4.6 V (vs. Li/Li^+) in the 1st, 6th and 30th cycle. As shown in Fig. 11a and b, the Nyquist plots for both electrodes are all composed of a depressed semi-circle in the high to medium frequency region and a quasi-straight line in the low frequency region. An equivalent circuit model is utilized to fit the experimental results, as can be seen in Fig. 11c. Generally, the high to medium frequency semi-circle is assigned to the charge transfer resistance (R_{ct}) in the electrode/electrolyte interface [41]. The low frequency tail is related to the Warburg impedance which signifies the impedance of lithium ion diffusion in bulk electrode material [42]. In addition, R_s represents the solution resistance, CPE (constant phase element) refers to the non-ideal double-layer capacitance, W_o indicates the Warburg impedance. As described in Table 1, the R_s values for both electrodes have no distinct changes during cycling process, which can be ascribed to the slow decomposition of electrolyte solution with cycles. Contrarily, the two electrodes both demonstrate increasing R_{ct} values upon cycling. This phenomenon can be associated to the fact that the thicker solid electrolyte interphase (SEI) film on the electrode surface increases the electrochemical kinetics obstacles. It can be seen, at the 1st cycle, that the CeF_3-coated $Li[Li_{0.2}Mn_{0.54}Ni_{0.13}Co_{0.13}]O_2$ electrode shows a

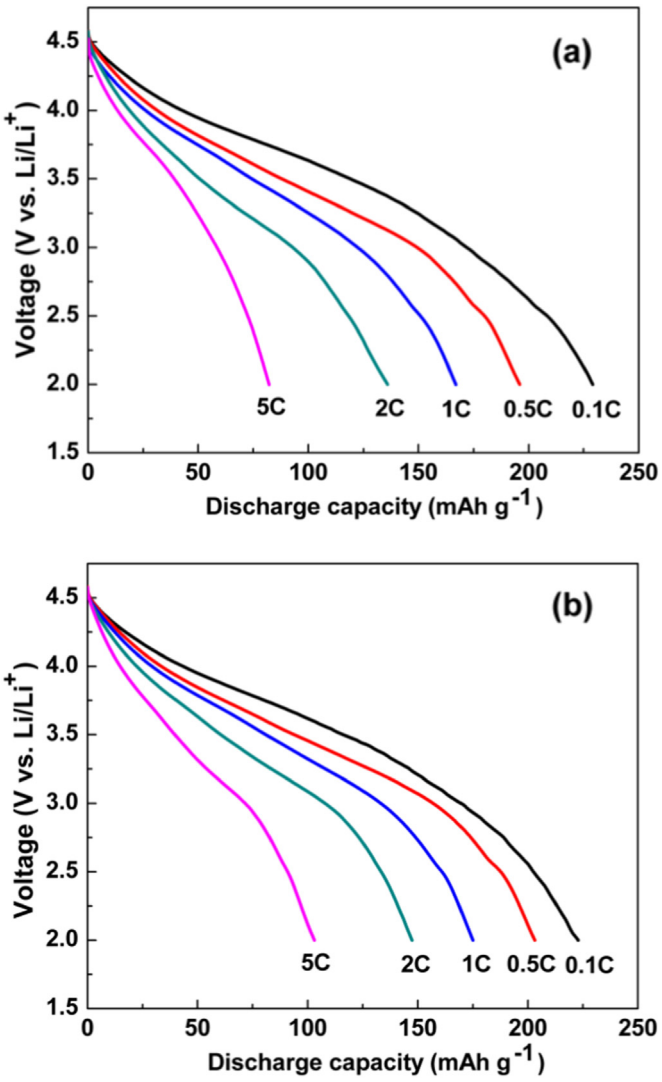

Fig. 10. The initial discharge profiles of (a) $Li[Li_{0.2}Mn_{0.54}Ni_{0.13}Co_{0.13}]O_2$ and (b) CeF_3-coated $Li[Li_{0.2}Mn_{0.54}Ni_{0.13}Co_{0.13}]O_2$ at a series of current densities.

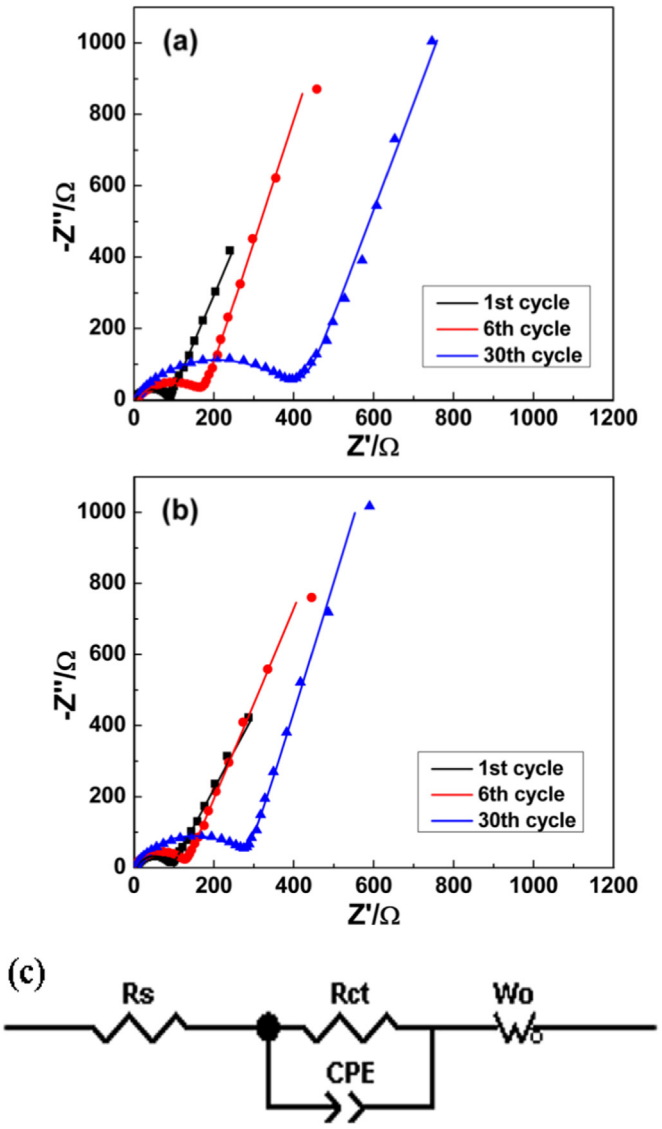

Fig. 11. Nyquist plots of (a) $Li[Li_{0.2}Mn_{0.54}Ni_{0.13}Co_{0.13}]O_2$ and (b) CeF_3-coated $Li[Li_{0.2}Mn_{0.54}Ni_{0.13}Co_{0.13}]O_2$ electrodes at a charge state of 4.6 V in the 1st, 6th, and 30th cycle and (c) the equivalent circuit used to fit the measured impedance spectra.

charge transfer resistance of 87.35 Ω, closing to the R_{ct} value (84.14 Ω) exhibited by the pristine cathode. This tiny difference of R_{ct} values between the two electrodes can be related to the insufficient interfacial contact between active material and electrolyte solution during the initial cycling process, resulting in only a slight protective effect against the electrolytic corrosion of electrode by coating CeF_3 on the surface of electrode. The result is consistent with the above analysis which represents unobvious electrochemical polarization for both electrodes during the initial charge–discharge process as shown in Fig. 7. However, the difference of R_{ct} values between the two electrodes becomes larger and larger as the cycle goes on. The ever-growing interface reaction between the electrolyte and electrode can be significantly responsible for the increase of R_{ct} values. As listed in Table 1, the R_{ct} value of the pristine cathode increases from 137.85 Ω at the 6th cycle to 362.63 Ω at the 30th cycle while the R_{ct} value of the CeF_3-coated is 124.81 Ω at the 6th cycle and reaches up to 281.12 Ω at the 30th cycle, showing a much smaller resistance increase than that of the pristine electrode. It can be speculated that CeF_3 acts as a role of a protective layer to restrain the oxidation of electrolyte and structural destruction of electrode material at high voltage so as to avoid the over-rapid thickening of electronically insulating SEI film which contains surface species such as polycarbonates, LiF, Li_xPF_y and $Li_xPO_yF_z$ [43], and decrease the rate of impedance increase during extensive cycling. Thus, enhanced electrochemcial performance for $Li[Li_{0.2}Mn_{0.54}Ni_{0.13}Co_{0.13}]O_2$ electrode can be obtained by surface coating with CeF_3.

The cyclic voltammetric profiles of both samples are shown in Fig. 12. It can be clearly seen that the CeF_3-coated electrode presents sharper and more symmetric redox peaks than the pristine one. Moreover, the peaks for both electrodes become less sharp

Table 1
The values of R_s and R_{ct} for pristine and CeF_3-coated $Li[Li_{0.2}Mn_{0.54}Ni_{0.13}Co_{0.13}]O_2$ after the 1st, 6th and 30th cycles.

Samples	R_s/Ω			R_{ct}/Ω		
	1st	6th	30th	1st	6th	30th
Pristine $Li[Li_{0.2}Mn_{0.54}Ni_{0.13}Co_{0.13}]O_2$	3.25	6.86	2.12	84.14	137.85	362.63
2 wt.% CeF_3-coated $Li[Li_{0.2}Mn_{0.54}Ni_{0.13}Co_{0.13}]O_2$	5.62	1.88	1.41	87.35	124.81	281.12

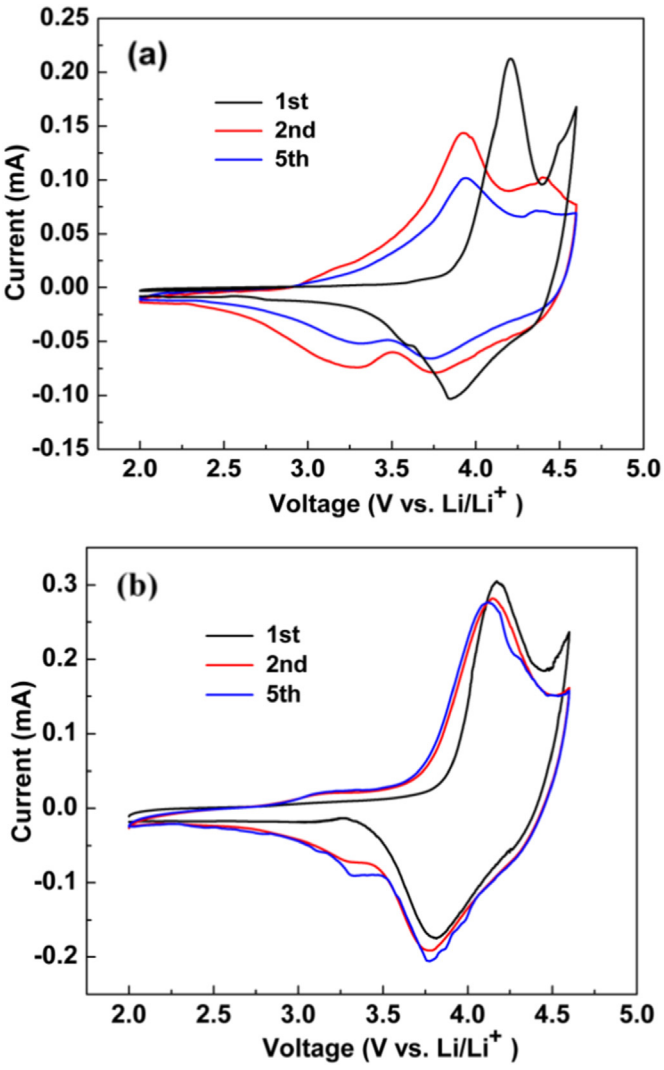

Fig. 12. The cyclic voltammetric profiles of (a) $Li[Li_{0.2}Mn_{0.54}Ni_{0.13}Co_{0.13}]O_2$ and (b) CeF_3-coated $Li[Li_{0.2}Mn_{0.54}Ni_{0.13}Co_{0.13}]O_2$ electrode at the 1st, 2nd and 5th cycles between 2.0 and 4.6 V at a scanning rate of 0.1 mV s^{-1}.

upon cycling. It is well known that the reduction of redox-peak intensity is ascribed to the cation mixing during cycling process [44]. Accordingly, an increasing disorder of cations can occur as cycle goes on, which obstructs lithium ion intercalation/deintercalation, leading to an undesirable capacity fading. As shown in Fig. 12a and b, the two electrodes both exhibit two anodic peaks at ~4.2 V and ~4.55 V in the initial charging process. According to the previous reports [40], the first anodic peak at 4.2 V corresponds to lithium extraction and simultaneous oxidation of Ni^{2+} to Ni^{4+} followed by Co^{3+} to Co^{4+}, while this peak shifts from 4.2 V to a lower potential (3.9–4.1 V) in later cycles, implying that the bulk material structure and/or the electrolyte/electrode interface may have been somewhat modified after the first electrochemcial cycling [45,46]. The second peak at ~4.55 V, corresponding to the long voltage plateau in the initial charge process, as shown in Fig. 7, can be ascribed to the extraction of lithium and escape of oxygen from the host lattices of layered Li_2MnO_3 region. Specially, owing to irreversible electrochemical reaction in the first cycle, the 4.55 V anodic peaks for both electrodes are not present in the followed cycles. Moreover, the cathodic peaks at about 3.8 V for the two electrodes are mainly due to the reduction of Ni^{4+} to Ni^{2+}. Generally, the cathodic peak at about 3.3 V does not appear in the initial discharge process [47,48]. However, in the 2nd and 5th cycles, this cathodic peak can be markedly observed, which indicates the reduction of Mn^{4+} in the layered MnO_2 component originating from the activation of electrochemically inactive Li_2MnO_3 domains, and also manifests good reversibility of Mn^{4+}/Mn^{3+} redox reaction. Compared with the 3.3 V cathodic peak in the 1st cycle, these sharper cathodic peaks in the 2nd and 5th cycles denominate easier reduction of Mn^{4+}/Mn^{3+} after activation of Li_2MnO_3 component during the 1st cycle. The CV curves of the CeF_3-coated electrode in the 2nd and 5th cycles show a better overlapping degree than that of the pristine sample, suggesting a more excellent reversibility of electrochemical redox due to the effective suppression of decomposition of electrolyte and dissolution of transition metal ions by surface coating with CeF_3 on the $Li[Li_{0.2}Mn_{0.54}Ni_{0.13}Co_{0.13}]O_2$ cathode material, which agrees well with the improved cyclic stability as shown in Fig. 8. Additionally, compared with the pristine $Li[Li_{0.2}Mn_{0.54}Ni_{0.13}Co_{0.13}]O_2$, the surface-coated electrode is subjected to weaker polarization due to the formed thinner and more appropriate SEI film, which can be expected to facilitate the diffusion of lithium ions. As a result, the CeF_3-coated electrode demonstrates a more superior rate capability than the pristine electrode upon cycling, as can be seen in Fig. 10.

4. Conclusions

In summary, the Li-rich layered $Li[Li_{0.2}Mn_{0.54}Ni_{0.13}Co_{0.13}]O_2$ electrode coated with CeF_3 was successfully prepared, and the electrochemical performance was also demonstrated in detail. The surface of the layered oxide was uniformly covered by an amorphous CeF_3 thin layer (~10 nm thick) using a simple chemical deposition method. The CeF_3 coating could improve the structural stability of $Li[Li_{0.2}Mn_{0.54}Ni_{0.13}Co_{0.13}]O_2$ electrode material, minimize the undesirable side reaction between the electrode and electrolyte, and suppress the increase of electrochemical impedance during cycling. By surface modification with CeF_3, the coated $Li[Li_{0.2}Mn_{0.54}Ni_{0.13}Co_{0.13}]O_2$ cathode displayed a significantly enhanced high-rate capability and cycling stability by restricting the over-rapid thickening of electronically insulating SEI film and inhibiting the damage of electrode structure, respectively. Therefore, surface coating with appropriate amount of CeF_3 will be a promising approach to obtain Li-rich layered oxide cathode materials with improved electrochemical performance for lithium-ion batteries.

Acknowledgments

This work was financially supported by the National Basic Research Program of China (973 program no. 2013CB934700).

References

[1] W. Tang, L.L. Liu, S. Tian, L. Li, Y.B. Yue, Y.P. Wu, S.Y. Guan, K. Zhu, Electrochem. Commun. 12 (2010) 1524–1526.
[2] S. Zhao, Y. Bai, Q.J. Chang, Y.Q. Yang, W.F. Zhang, Electrochim. Acta 108 (2013) 727–735.
[3] Y.Y. Liu, C.B. Cao, J. Li, Electrochim. Acta 55 (2010) 3921–3926.
[4] S.Y. Chung, J.T. Bloking, Y.M. Chiang, Nat. Mater. 1 (2002) 123–128.
[5] P.P. Prosini, M. Lisi, D. Zane, M. Pasquali, Solid State Ionics 148 (2002) 45–51.
[6] A. Ito, D.C. Li, Y. Ohsawa, Y. Sato, J. Power Sources 183 (2008) 344–346.
[7] G.Z. Wei, X. Lu, F.S. Ke, L. Huang, J.T. Li, Z.X. Wang, Z.Y. Zhou, S.G. Sun, Adv. Mater. 22 (2010) 4364–4367.
[8] J.R. Croy, D.H. Kim, M. Balasubramanian, K. Gallagher, S.-H. Kang, M.M. Thackeray, J. Electrochem. Soc. 159 (2012) 781–790.
[9] J. Zheng, S.N. Deng, Z.C. Shi, H.J. Xu, H. Xu, Y.F. Deng, Z.C. Zhang, G.H. Chen, J. Power Sources 221 (2013) 108–113.
[10] J. Gao, J. Kim, A. Manthiram, Electrochem. Commun. 11 (2009) 84–86.
[11] J. Li, R. Klöpsch, M.C. Stan, S. Nowak, M. Kunze, M. Winter, S. Passerini, J. Power Sources 196 (2011) 4821–4825.

[12] Z.J. He, Z.X. Wang, H.J. Guo, X.H. Li, X.W. Wu, P. Yue, J.X. Wang, Mater. Lett. 91 (2013) 261–264.
[13] S.K. Martha, J. Nanda, G.M. Veith, N.J. Dudney, J. Power Sources 199 (2012) 220–226.
[14] Y.-S. Hong, Y.J. Park, K.S. Ryu, S.H. Chang, M.G. Kim, J. Mater. Chem. 14 (2004) 1424–1429.
[15] M. Gu, I. Belharouak, J.M. Zheng, H.M. Wu, J. Xiao, A. Genc, K. Amine, S. Thevuthasan, D.R. Baer, J.-G. Zhang, N.D. Browning, J. Liu, C.M. Wang, ACS Nano 7 (2013) 760–767.
[16] S.J. Shi, J.P. Tu, Y.J. Zhang, Y.D. Zhang, X.Y. Zhao, X.L. Wang, C.D. Gu, Electrochim. Acta 108 (2013) 441–448.
[17] X.Y. Liu, J.L. Liu, T. Huang, A.S. Yu, Electrochim. Acta 109 (2013) 52–58.
[18] S.-T. Myung, K. Izumi, S. Komaba, Y.-K. Sun, H. Yashiro, N. Kumagai, Chem. Mater. 17 (2005) 3695–3704.
[19] Y.P. Chen, Y. Zhang, B.J. Chen, Z.Y. Wang, C. Lu, J. Power Sources 256 (2014) 20–27.
[20] G. Singh, R. Thomas, A. Kumar, R.S. Katiyar, A. Manivannan, J. Electrochem. Soc. 159 (2012) 470–478.
[21] E.S. Han, Y.P. Li, L.Z. Zhu, L. Zhao, Solid State Ionics 255 (2014) 113–119.
[22] Z.Y. Wang, E.Z. Liu, L.C. Guo, C.S. Shi, C.N. He, J.J. Li, N.Q. Zhao, Surf. Coat. Technol. 235 (2013) 570–576.
[23] J.M. Zheng, Z.R. Zhang, X.B. Wu, Z.X. Dong, Z. Zhu, Y. Yang, J. Electrochem. Soc. 155 (2008) 775–782.
[24] G.R. Li, X. Feng, Y. Ding, S.H. Ye, X.P. Gao, Electrochim. Acta 78 (2012) 308–315.
[25] J.-H. Kim, M.-S. Park, J.-H. Song, D.-J. Byun, Y.-J. Kim, J.-S. Kim, J. Alloys Compd. 517 (2012) 20–25.
[26] F. Amalraj, M. Talianker, B. Markovsky, L. Burlaka, N. Leifer, G. Goobes, E.M. Erickson, O. Haik, J. Grinblat, E. Zinigrad, D. Aurbach, J.K. Lampert, J.-Y. Shin, M. Schulz-Dobrick, A. Garsuch, J. Electrochem. Soc. 160 (2013) 2220–2233.
[27] F. Wu, M. Wang, Y.F. Su, L.Y. Bao, S. Chen, Electrochim. Acta 54 (2009) 6803–6807.
[28] D. Arumugam, G. Paruthimal Kalaignan, Electrochim. Acta 55 (2010) 8709–8716.
[29] H.-W. Ha, N.J. Yun, M.H. Kim, M.H. Woo, K. Kim, Electrochim. Acta 51 (2006) 3297–3302.
[30] Y. Liu, C.H. Mi, C.Z. Yuan, X.G. Zhang, J. Electroanal. Chem. 628 (2009) 73–80.
[31] H.-W. Ha, K.H. Jeong, N.J. Yun, M.Z. Hong, K. Kim, Electrochim. Acta 50 (2005) 3764–3769.
[32] B.L. Han, X.C. Lu, Surf. Coat. Technol. 203 (2009) 3656–3660.
[33] D. ArunKumar, S. Selvasekarapandian, H. Nithya, Y. Masuda, Solid State Sci. 14 (2012) 626–634.
[34] A.K. Dorai, S. Subramanian, N. Hellar, Mater. Chem. Phys. 143 (2014) 765–772.
[35] D. Mohanty, S. Kalnaus, R.A. Meisner, K.J. Rhodes, J.L. Li, E.A. Payzant, D.L. Wood III, C. Daniel, J. Power Sources 229 (2013) 239–248.
[36] Y.H. Deng, S.Q. Liu, X.X. Liang, J. Solid State Electrochem. 17 (2013) 1067–1075.
[37] S.-H. Kang, M.M. Thackeray, Electrochem. Commun. 11 (2009) 748–751.
[38] J.M. Zheng, J. Li, Z.R. Zhang, X.J. Guo, Y. Yang, Solid State Ionics 179 (2008) 1794–1799.
[39] W.C. Choi, A. Benayard, J.-H. Park, J.H. Park, S.-G. Doo, J.Y. Mun, Electrochim. Acta 117 (2014) 492–497.
[40] J.Q. Zhao, S. Aziz, Y. Wang, J. Power Sources 247 (2014) 95–104.
[41] S.J. Shi, J.P. Tu, Y.J. Mai, Y.Q. Zhang, C.D. Gu, X.L. Wang, Electrochim. Acta 63 (2012) 112–117.
[42] J.M. Zheng, X.B. Wu, Y. Yang, Electrochim. Acta 56 (2011) 3071–3078.
[43] S.K. Martha, J. Nanda, G.M. Veith, N.J. Dudney, J. Power Sources 216 (2012) 179–186.
[44] K. Karthikeyan, S. Amaresh, G.W. Lee, V. Aravindan, H. Kim, K.S. Kang, W.S. Kim, Y.S. Lee, Electrochim. Acta 68 (2012) 246–253.
[45] G.M. Koenig Jr., I. Belharouak, H.M. Wu, K. Amine, Electrochim. Acta 56 (2011) 1426–1431.
[46] X. Wei, S.C. Zhang, Z.J. Du, P.H. Yang, J. Wang, Y.B. Ren, Electrochim. Acta 107 (2013) 549–554.
[47] Y.-K. Sun, M.-J. Lee, C.S. Yoon, J. Hassoun, K. Amine, B. Scrosati, Adv. Mater. 24 (2012) 1192–1196.
[48] S.-H. Kang, Y.K. Sun, K. Amine, Electrochem. Solid-State Lett. 6 (2003) 183–186.